

Enhancement of temperature of quantum anomalous Hall effect in two-dimensional germanene/magnetic semiconductor heterostructures

Qing-Han Yang,¹ Jia-Wen Li,¹ Xin-Wei Yi,² Xiang Li,¹ Jing-Yang You,³ Gang Su,^{1,2,4,5,*} and Bo Gu^{1,5,†}

¹*Kavli Institute for Theoretical Sciences, University of Chinese Academy of Sciences, Beijing 100049, China*

²*School of Physical Sciences, University of Chinese Academy of Sciences, Beijing 100049, China*

³*Peng Huanwu Collaborative Center for Research and Education, Beihang University, Beijing 100191, China*

⁴*Institute of Theoretical Physics, Chinese Academy of Sciences, Beijing 100190, China*

⁵*Physical Science Laboratory, Huairou National Comprehensive Science Center, Beijing 101400, China*

Quantum anomalous Hall effect (QAHE) is significant for future low-power electronics devices, where a main challenge is realizing QAHE at high temperatures. In this work, based on experimentally reported two-dimensional (2D) germanene and magnetic semiconductors $\text{Cr}_2\text{Ge}_2\text{Te}_6$ and $\text{Cr}_2\text{Si}_2\text{Te}_6$, and the first principle calculations, germanene/magnetic semiconductor heterostructures are investigated. Topologically nontrivial edge states and quantized anomalous Hall conductance are demonstrated. It is shown that the QAHE temperature can be enhanced to approximately 62 K in germanene/monolayer (ML) $\text{Cr}_2\text{Ge}_2\text{Te}_6$ with 2.1% tensile strain, 64 K in germanene/bilayer (BL) $\text{Cr}_2\text{Ge}_2\text{Te}_6$ with 1.4% tensile strain, and 50 K in germanene/ML $\text{Cr}_2\text{Si}_2\text{Te}_6$ with 1.3% tensile strain. With increasing tensile strain of these heterostructures, the band gap decreases and the Curie temperature rises, and the highest temperature of QAHE is obtained. Since these 2D materials were discovered in recent experiments, our results provide promising materials for achieving high-temperature QAHE.

I. INTRODUCTION

Quantum anomalous Hall effect (QAHE) is one of the most exciting phenomenon of matter and is characterized by an integer Chern number \mathcal{C} [1, 2]. A key manifestation of QAHE is the dissipationless chiral edge current. It has the potential to revolutionize future low-power quantum electronic devices. Therefore, much theoretical and experimental research has been conducted to achieve QAHE at high temperatures [3–26]. Various methods are being explored to achieve QAHE. Introducing ferromagnetic order in topological insulators (TIs) is a primary method for achieving QAHE. The first observation of QAHE occurred in magnetically doped TIs, i.e., Cr-doped $(\text{Bi,Sb})_2\text{Te}_3$ thin films at 30 mK [3]. Subsequent research has focused on increasing the QAHE temperature. For example, the anomalous Hall resistance ρ_{xy} reaches a maximum value of $0.95h/e^2$ in a 10 quintuple-layer (QL) thin film of $\text{Cr}_{0.1}(\text{Bi}_{0.5},\text{Sb}_{0.5})_{1.9}\text{Te}_3$ at 280 mK [8], and a six QL $(\text{Cr}_{0.12}\text{Bi}_{0.26}\text{Sb}_{0.62})_2\text{Te}_3$ film exhibits a quantized anomalous Hall resistance R_{yx} up to 0.3 K [10]. To date, the highest reported record QAHE temperature in these doped magnetic TIs is approximately 2 K [11]. Because disordered magnetic impurities can inevitably degrade sample quality, thus limiting the QAHE temperature. Many researchers are investigating intrinsic QAHE materials. In recent years, experimental breakthroughs in QAHE have been achieved in the van der Waals (vdW) layered material MnBi_2Te_4 [12–14]. MnBi_2Te_4 is a layered magnetic TI consisting of Te-Bi-Te-Mn-Te-Bi-Te septuple layers (SLs) with antiferromag-

netic ground state characterized by antiferromagnetic interlayer coupling and ferromagnetic intralayer coupling. In five SL flakes, the quantization temperature can be increased to 6.5 K by aligning all layers ferromagnetically with an external magnetic field [12]. Recent studies have revealed the QAHE in moiré materials can be derived from both graphene [21–23] and transition-metal dichalcogenides (TMDs) [24]. In these systems, QAHE originates from spontaneous valley polarization. However, the typically small band gap of such systems imposes significant limitations on the realization temperature of the QAHE [25, 26].

Another approach to achieving the QAHE state involves fabricating TI/magnetic semiconductor heterostructures. Recent experimental evidence has shown that low-buckled epitaxial germanene is a quantum spin Hall insulator with a large bulk gap and robust metallic edges at 77 K [27]. The quantized spin Hall conductance has also been confirmed by first principle calculations [28]. Furthermore, two-dimensional (2D) $\text{Cr}_2\text{Ge}_2\text{Te}_6$ has been experimentally demonstrated as a ferromagnetic semiconductor, with a Curie temperature (T_C) of 28 K for bilayer (BL) $\text{Cr}_2\text{Ge}_2\text{Te}_6$ [29]. Previous theoretical studies suggest that chiral edge states and quantized Hall conductance can be realized in germanene/ $\text{Cr}_2\text{Ge}_2\text{Te}_6$ heterostructures [30, 31]. A key question is whether the QAHE temperature can be enhanced in germanene/monolayer (ML) $\text{Cr}_2\text{Ge}_2\text{Te}_6$. Recent studies have indicated that tensile strain is an effective method for increasing the T_C of 2D $\text{Cr}_2\text{Ge}_2\text{Te}_6$ [32, 33]. First-principles calculations predict a T_C of 144 K for ML $\text{Cr}_2\text{Ge}_2\text{Te}_6$ under 5% tensile strain [33]. Experimentally, strain can be applied to samples through various techniques [33–38], including using a micro-manipulator on the substrate to transfer strain to the sample [34] or exploiting lattice mismatch between differ-

* gsu@ucas.ac.cn

† gubo@ucas.ac.cn

ent materials [35]. Gradient-modulated strain up to 4% has been reported in experiments with vdW heterostructures [38].

In this paper, we report our first-principles study on enhancing the QAHE temperature in germanene/magnetic semiconductor heterostructures. We investigated the effect of biaxial tensile strain on these heterostructures to increase the QAHE temperature. Our calculations show that a QAHE temperature of 62 K is achieved in the germanene/ML $\text{Cr}_2\text{Ge}_2\text{Te}_6$ heterostructure with 2.1% tensile strain. For the germanene/BL $\text{Cr}_2\text{Ge}_2\text{Te}_6$ heterostructure, a QAHE temperature of 64 K is obtained with 1.4% tensile strain, while the germanene/ML $\text{Cr}_2\text{Si}_2\text{Te}_6$ heterostructure exhibits a QAHE temperature of 50 K under 1.3% tensile strain. These results suggest a promising route for achieving high-temperature QAHE using experimentally available 2D materials.

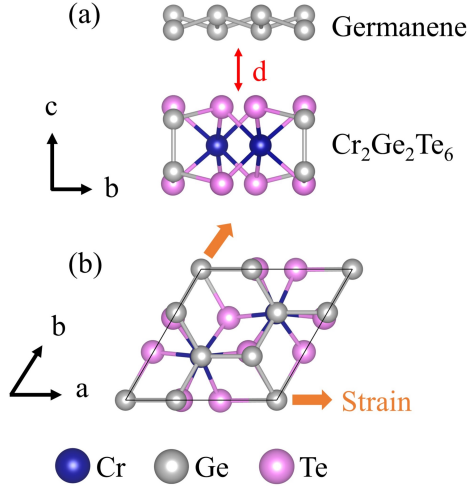


FIG. 1. Crystal structures of two-dimensional germanene/ML $\text{Cr}_2\text{Ge}_2\text{Te}_6$ heterostructure: (a) side view, and (b) top view, respectively. The arrows indicate biaxial tensile strain applied to the heterostructure.

II. METHOD

Our first-principle calculations are based on Vienna *ab initio* simulation package (VASP) [39]. We chose the Perdew-Burke-Ernzerhof (PBE) form with the generalized gradient approximation (GGA) to describe the exchange-correlation potential [40]. The DFT-D3 method is adopted to describe the vdW interaction between germanene and magnetic semiconductor layers [41]. The vacuum length is taken as 20 Å, which is enough to isolate the present two-dimensional (2D) system. Spin-orbit coupling (SOC) is taken into account in the calculations. It is reasonable to adopt Hubbard $U = 4$ eV for 3d electrons of Cr in ML $\text{Cr}_2\text{Ge}_2\text{Te}_6$ [42].

The $12 \times 12 \times 1$ Γ -center k point is used for the Brillouin zone (BZ) sampling. All the structures were fully relaxed with the convergence precision of energy and force of 10^{-7} eV and 10^{-3} eV/Å, respectively. The Wannier90 code was used to construct a tight-binding Hamiltonian [43, 44] and WannierTools code was used to obtain topological properties of band [45].

III. QAHE IN GERMANENE/ML $\text{Cr}_2\text{Ge}_2\text{Te}_6$ HETEROSTRUCTURE

The crystal structure with the side and top views of the germanene/ML $\text{Cr}_2\text{Ge}_2\text{Te}_6$ heterostructure is shown in Fig. 1. The heterostructure is constructed using a $\sqrt{3} \times \sqrt{3}$ supercell of germanene and a 1×1 unit cell of ML $\text{Cr}_2\text{Ge}_2\text{Te}_6$ with an interlayer distance of $d = 3.45$ Å. The calculated lattice mismatch between germanene and $\text{Cr}_2\text{Ge}_2\text{Te}_6$ is less than 1%. The optimized in-plane lattice constant of the germanene/ $\text{Cr}_2\text{Ge}_2\text{Te}_6$ heterostructure is $a = 6.954$ Å, which is slightly smaller than that of the optimized ML $\text{Cr}_2\text{Ge}_2\text{Te}_6$ ($a = 6.964$ Å).

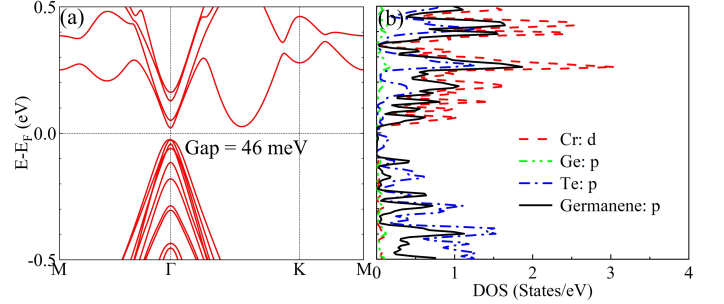


FIG. 2. (a) Electronic band structures and (b) density of states of germanene/ML $\text{Cr}_2\text{Ge}_2\text{Te}_6$ heterostructure obtained by the first principle calculations with SOC.

The electronic band structures and density of states (DOS) of germanene/ML $\text{Cr}_2\text{Ge}_2\text{Te}_6$ heterostructure are shown in Fig. 2. With SOC included, the germanene/ML $\text{Cr}_2\text{Ge}_2\text{Te}_6$ heterostructure exhibits a finite band gap of 46 meV. This indicates that even at room temperature, thermal fluctuations are insufficient to fully populate the band gap. The Dirac cone around the Γ point is predominantly contributed by p_z orbits of germanene. Notably, this band gap is larger than that of pristine germanene. Since SOC depends on the atomic number ($\sim Z^4$) and SOC strength of Te is larger than that of germanene, the observed band gap enhancement is attributed to interlayer coupling and hybridization. To investigate the topological properties, maximally localized Wannier functions (MLWFs) implemented in the Wannier90 code were used to fit our density functional theory (DFT) band calculations. The anomalous Hall conductivity is calculated using $\sigma_{xy} = \mathcal{C} \frac{e^2}{h}$, where \mathcal{C} is the Chern

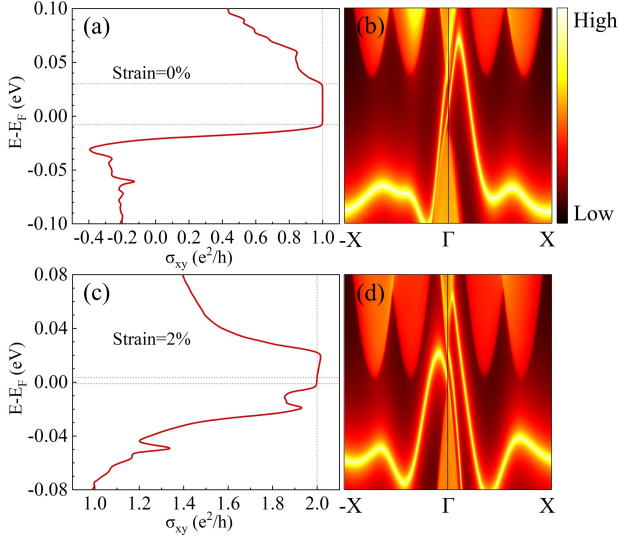


FIG. 3. For germanene/ML $\text{Cr}_2\text{Ge}_2\text{Te}_6$ heterostructure, (a) anomalous Hall conductivity and (b) chiral edge states near the Fermi level for the case without strain. (c)-(d) for the case with 2% tensile strain.

number defined as

$$\mathcal{C} = \frac{1}{2\pi} \int_{BZ} \Omega(\mathbf{k}) d\mathbf{k}, \quad (1)$$

and $\Omega(\mathbf{k})$ is the Berry curvature that can be obtained as

$$\Omega(\mathbf{k}) = - \sum_{n < E_F} \sum_{m \neq n} 2Im \frac{\langle \psi_{n\mathbf{k}} | v_x | \psi_{m\mathbf{k}} \rangle \langle \psi_{m\mathbf{k}} | v_y | \psi_{n\mathbf{k}} \rangle}{(\epsilon_{m\mathbf{k}} - \epsilon_{n\mathbf{k}})^2}, \quad (2)$$

where $\psi_{m(n)\mathbf{k}}$ are the Bloch wave functions. $\epsilon_{m(n)\mathbf{k}}$ are the eigenvalues and $v_{x(y)}$ are the velocity operators. Such calculation has been implemented in the WannierTools code [45]. The calculated Chern number for the valence band near the Fermi level is $\mathcal{C} = 1$, confirming the topologically nontrivial nature of the band structure. Fig. 3(a) shows the calculated anomalous Hall conductance as a function of chemical potential, revealing a quantized Hall plateau at $\sigma_{xy} = \frac{e^2}{h}$. The plateau is consistent with the presence of one topologically nontrivial edge state connecting the bulk states in Fig. 3(b).

To investigate magnetic properties of this heterostructure, we considered the following Heisenberg-type Hamiltonian:

$$H = \sum_{\langle i,j \rangle} J_1 \mathbf{S}_i \cdot \mathbf{S}_j + \sum_{\langle\langle i,j \rangle\rangle} J_2 \mathbf{S}_i \cdot \mathbf{S}_j + \sum_{\langle\langle\langle i,j \rangle\rangle\rangle} J_3 \mathbf{S}_i \cdot \mathbf{S}_j + M \sum_i (S_i^z)^2, \quad (3)$$

where J_1 , J_2 , J_3 denote the nearest neighbor, second-nearest-neighbor and third-nearest-neighbor exchange

couplings, respectively. To determine the magnetization direction, we performed total-energy calculations for both out-of plane and in-plane magnetization. Our results show that the easy axis is perpendicular to the 2D plane, consistent with experimental results for 2D $\text{Cr}_2\text{Ge}_2\text{Te}_6$ [29]. To obtain exchange couplings, we considered four spin configurations: ferromagnetic (FM), Neel antiferromagnetic (AFM), Stripy AFM and Zigzag AFM as shown in Fig. 4(a). The energy of four configurations are expressed as

$$\begin{aligned} E_{FM} &= 12J_1 + 24J_2 + 12J_3 + E_0, \\ E_{NAFM} &= -12J_1 + 24J_2 - 12J_3 + E_0, \\ E_{SAFM} &= -4J_1 - 8J_2 + 12J_3 + E_0, \\ E_{ZAFM} &= 4J_1 - 8J_2 - 12J_3 + E_0, \end{aligned} \quad (4)$$

where E_0 is the energy which is independent of the spin configurations. J_1 , J_2 , J_3 are provided in supplementary materials (SMs) [46]. The Monte Carlo (MC) simulations were performed on a $20 \times 20 \times 1$ hexagonal lattice with periodic boundary conditions, using 10^6 MC steps per temperature. The resulting temperature dependence of the magnetization and susceptibility for unstrained germanene/ML $\text{Cr}_2\text{Ge}_2\text{Te}_6$ heterostructure is presented in Fig. 4(b).

To investigate the effect of tensile strain on the critical temperature of germanene/ $\text{Cr}_2\text{Ge}_2\text{Te}_6$ heterostructure, biaxial tensile strain was applied. Strain is defined as $(a - a_0)/a_0$, where a and a_0 are the lattice constants with and without strain, respectively. As shown in Fig. 4(c), T_C increases with strain. To address the overestimation of T_C by MC results, a rescaling method was employed. The calculated T_C^{MC} of 50 K for ML $\text{Cr}_2\text{Ge}_2\text{Te}_6$ without strain was scaled to match the experimental T_C of 28 K for 2D $\text{Cr}_2\text{Ge}_2\text{Te}_6$ [29]. All T_C^{MC} values for strained germanene/ML $\text{Cr}_2\text{Ge}_2\text{Te}_6$ and ML $\text{Cr}_2\text{Ge}_2\text{Te}_6$ were then normalized by the unstrained ML $\text{Cr}_2\text{Ge}_2\text{Te}_6$ T_C^{MC} of 50 K. These ratios were subsequently multiplied by 28 K to provide more reliable T_C estimates as shown in Fig. 4(c).

As shown in Fig. 5, increasing tensile strain in germanene/ML $\text{Cr}_2\text{Ge}_2\text{Te}_6$ heterostructure leads to an increase in T_C and a decrease in the band gap. The gap nearly closes at a tensile strain of 2.4%. The band gap have been given in unit of K. The yellow region in Fig. 5 indicates the predicted QAHE phase. Notably, a QAHE state is predicted up to 62 K in the germanene/ML $\text{Cr}_2\text{Ge}_2\text{Te}_6$ heterostructure with 2.1% tensile strain.

To understand the decrease in band gap with increasing tensile strain, we analyzed the fatband structure around the Fermi level for germanene/ML $\text{Cr}_2\text{Ge}_2\text{Te}_6$ heterostructure at strain=0% and strain=2% as shown in Fig. 6. Clearly, the bands around Γ point are mainly contributed by p_z orbitals of germanene, while those along the $\Gamma - K$ path are dominated by d_{xz} and d_{yz} orbitals of Cr. In the unstrained heterostructure, the direct band gap is located at Γ . With increasing tensile strain, the bands at Γ show little variation, but the bands along

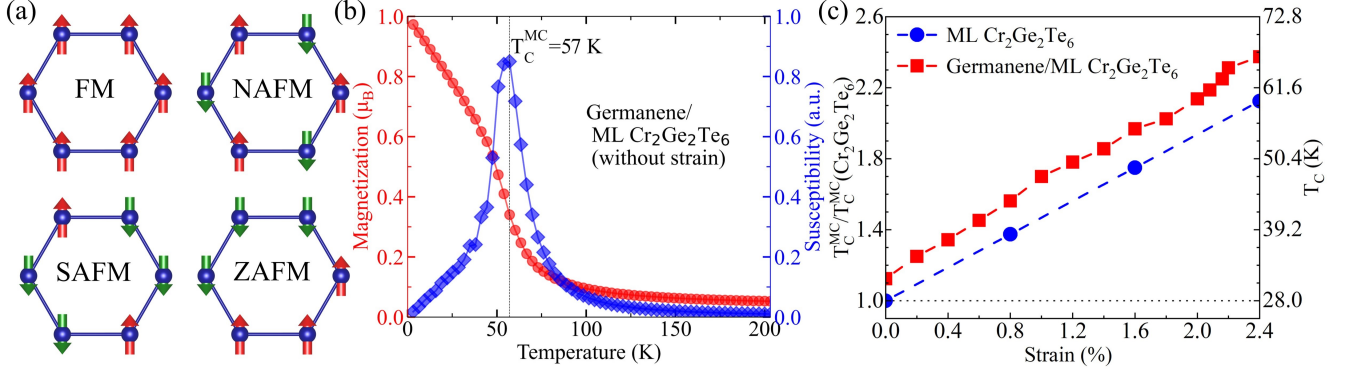


FIG. 4. (a) Four different spin configurations for Cr atoms in the honeycomb lattice: FM (ferromagnetic), Neel AFM (antiferromagnetic), Stripy AFM and Zigzag AFM. Red and green arrows represent the Cr atom with spin up and spin down polarizations, respectively. (b) The calculated magnetization and susceptibility as a function of temperature for germanene/ $\text{Cr}_2\text{Ge}_2\text{Te}_6$ heterostructure without applying strain by MC simulations, where the Curie temperature is obtained as $T_C^{\text{MC}} = 57$ K. (c) The rescaled Curie temperature T_C as a function of tensile strain by MC simulations for germanene/ML $\text{Cr}_2\text{Ge}_2\text{Te}_6$ heterostructure and ML $\text{Cr}_2\text{Ge}_2\text{Te}_6$. See text for details.

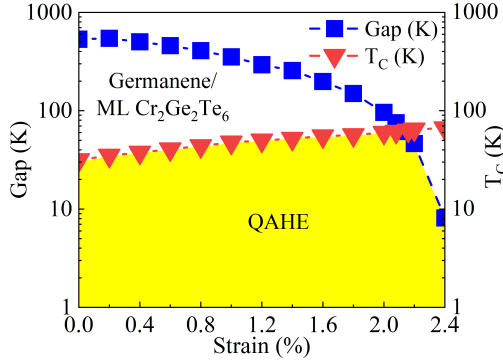


FIG. 5. The band gap and Curie temperature T_C as a function of tensile strain of germanene/ML $\text{Cr}_2\text{Ge}_2\text{Te}_6$ heterostructure.

$\Gamma - K$ shift downwards, resulting in a reduced band gap.

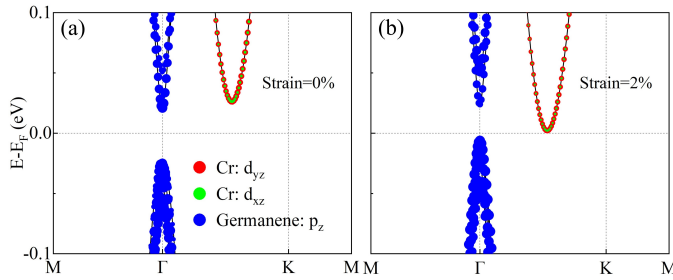


FIG. 6. The fatband around the Fermi level of germanene/ML $\text{Cr}_2\text{Ge}_2\text{Te}_6$ heterostructure (a) without strain and (b) with 2% tensile strain.

The great enhancement of T_C in germanene/ML $\text{Cr}_2\text{Ge}_2\text{Te}_6$ heterostructure under tensile strain can be explained by considering the superexchange interaction [47–49]. The superexchange interaction involves two pro-

cesses. One is the direct exchange process between the d_2 electrons of the Cr_2 atom and the p' electrons of the Te atom, presented by $J_{p'd_2}$. The other is the hopping process between the p electrons of the Te atom and the d_1 electrons of the Cr1 atom, presented by V_{pd_1} . The coupling J_{super} between the two Cr atoms can be expressed as [46]

$$J_{\text{super}} = \frac{1}{4} \sum_{d_1, p, p', d_2} |V_{pd_1}|^2 J_{p'd_2} \left[\frac{1}{(E_{d_1 d_1}^{\uparrow\uparrow})^2} - \frac{1}{(E_{d_1 d_1}^{\uparrow\downarrow})^2} \right].$$

$$= \frac{1}{4A} \sum_{d_1, p, p', d_2} |V_{pd_1}|^2 J_{p'd_2}, \quad (5)$$

where $A \equiv 1/(1/(E_{d_1 d_1}^{\uparrow\uparrow})^2 - 1/(E_{d_1 d_1}^{\uparrow\downarrow})^2)$ is taken as a pending parameter and does not change with strain. $E_{d_1 d_1}^{\uparrow\uparrow}$ and $E_{d_1 d_1}^{\uparrow\downarrow}$ are energies of two d electrons at the same Cr atom with parallel and antiparallel spins, respectively. V_{pd_1} is the hopping parameter between the p electrons and the d_1 electrons. The direct p - d exchange $J_{p'd_2}$ can be derived from the s - d exchange model following the Schrieffer-Wolff transformation [50]

$$J_{p'd_2} = 2|V_{p'd_2}|^2 \left(\frac{1}{E_{p'} - E_{d_2}} + \frac{1}{E_{d_2} + U - E_{p'}} \right), \quad (6)$$

where $E_{p'}$ and E_{d_2} are the energy level of the p' electrons and the d_2 electrons, respectively. $V_{p'd_2}$ is the hopping parameter between the p' electrons and the d_2 electrons. These parameters can be obtained by DFT calculation and Wannier90 code.

Due to the crystal field, the d electron configuration of Cr is split into two groups: e_g (d_{z^2} and $d_{x^2-y^2}$ orbitals) and t_{2g} (d_{xz} , d_{yz} and d_{xy} orbitals). Wannier90 calculations indicate that the main contribution comes from e_g .

TABLE I. $|V_{pd1}|^2$ and $E_{p'} - E_{d2}$ between $5p$ orbitals of Te and d_{z^2} , $d_{x^2-y^2}$ orbitals of Cr for relaxed and strained ML $\text{Cr}_2\text{Ge}_2\text{Te}_6$ (in units of eV).

	Strain = 0%					
	$p_z - d_{z^2}$	$p_x - d_{z^2}$	$p_y - d_{z^2}$	$p_z - d_{x^2-y^2}$	$p_x - d_{x^2-y^2}$	$p_y - d_{x^2-y^2}$
$ V_{pd1} ^2$	1.539	0.439	0.051	8.5E-5	0.026	0.005
$E_{p'} - E_{d2}$	0.430	0.551	0.415	0.317	0.438	0.302
$J_{super}A$	16.33					
	Strain = 2%					
	$p_z - d_{z^2}$	$p_x - d_{z^2}$	$p_y - d_{z^2}$	$p_z - d_{x^2-y^2}$	$p_x - d_{x^2-y^2}$	$p_y - d_{x^2-y^2}$
$ V_{pd1} ^2$	1.407	0.425	0.065	1.5E-4	0.023	0.005
$E_{p'} - E_{d2}$	0.430	0.480	0.516	0.285	0.335	0.371
$J_{super}A$	18.43					

The values of $|V_{pd1}|^2$ and $E_{p'} - E_{d2}$ for the $\text{Cr}_1\text{-Te}_1\text{-Cr}_2$ path in ML $\text{Cr}_2\text{Ge}_2\text{Te}_6$ without and with tensile strain are listed in Table. I. The resulting superexchange interaction J_{super} for relaxed and strained ML $\text{Cr}_2\text{Ge}_2\text{Te}_6$ are $16.33/A$ and $18.43/A$, respectively. The ratio of J_{super} for strained to relaxed ML $\text{Cr}_2\text{Ge}_2\text{Te}_6$ is 1.13, which is comparable to the ratio (1.25) of the DFT-calculated nearest neighbor exchange coupling J_1 for the strained and relaxed germanene/ML $\text{Cr}_2\text{Ge}_2\text{Te}_6$ heterostructure. Comparison of the strained and unstrained ML $\text{Cr}_2\text{Ge}_2\text{Te}_6$ results reveals that the enhancement of the superexchange interaction J_{super} is primarily due to the decreased energy difference $E_{p'} - E_{d2}$. This decrease in $E_{p'} - E_{d2}$ contributes to the enhancement of both J_{super} and T_C . The Cr-Te-Cr bond angles are 89.8° and 91.2° for relaxed and strained ML $\text{Cr}_2\text{Ge}_2\text{Te}_6$, respectively, indicating no significant difference in the hopping parameter $|V_{pd1}|^2$ as shown in Table. I.

The application of strain could enhance the QAH transition temperature in the germanene/ML $\text{Cr}_2\text{Ge}_2\text{Te}_6$ heterostructure. Because T_C in 2D magnetic semiconductor $\text{Cr}_2\text{Ge}_2\text{Te}_6$ can be dramatically increased by strain, which has been demonstrated in recent experiment [33]. The fundamental mechanism lies in strain-induced reduction of the energy difference between anions and cations, which contributes to the enhancement of T_C by the superexchange mechanism. However, the application of strain simultaneously reduces the band gap of the heterostructure germanene/ML $\text{Cr}_2\text{Ge}_2\text{Te}_6$ by lowering the conduction bands. Consequently, the upper limit of the QAH temperature in germanene/ML $\text{Cr}_2\text{Ge}_2\text{Te}_6$ heterostructure is determined by the intersection of T_C and band gap curves.

IV. QAHE IN GERMANENE/BL $\text{Cr}_2\text{Ge}_2\text{Te}_6$ AND GERMANENE/ML $\text{Cr}_2\text{Si}_2\text{Te}_6$ HETEROSTRUCTURES

We also investigated the QAHE in germanene/BL $\text{Cr}_2\text{Ge}_2\text{Te}_6$ and germanene/ML $\text{Cr}_2\text{Si}_2\text{Te}_6$ heterostructures, and the results are shown in Fig. 7. Experiments have demonstrated an out-of-plane easy-axis and inter-

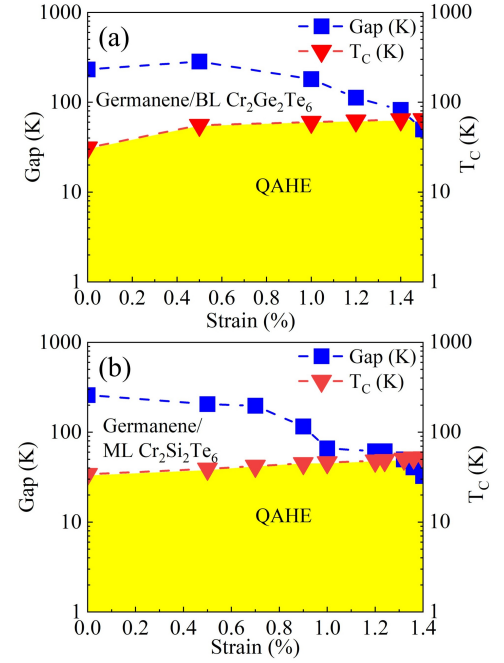


FIG. 7. The band gap and T_C as a function of tensile strain of (a) germanene/BL $\text{Cr}_2\text{Ge}_2\text{Te}_6$ and (b) germanene/ML $\text{Cr}_2\text{Si}_2\text{Te}_6$ heterostructures.

layer ferromagnetic coupling in BL $\text{Cr}_2\text{Ge}_2\text{Te}_6$ [29]. To determine an appropriate Hubbard U parameter, we calculated the magnetic anisotropy energy (MAE) ($E_{||} - E_{\perp}$) and the energy difference between AFM and FM interlayer configurations ($E_{AFM} - E_{FM}$) as a function of U . As shown in SMs, a value of $U = 1.3$ eV accurately reproduces the experimental observations for BL $\text{Cr}_2\text{Ge}_2\text{Te}_6$. Consequently, this value was adopted for germanene/BL $\text{Cr}_2\text{Ge}_2\text{Te}_6$ calculations. The SMs also present the four different spin configurations of Cr atoms to calculate the T_C of BL $\text{Cr}_2\text{Ge}_2\text{Te}_6$. Our calculations reveal that the germanene/BL $\text{Cr}_2\text{Ge}_2\text{Te}_6$ heterostructure exhibits the QAHE up to 64 K under a 1.4% tensile strain as shown in Fig. 7(a).

For the germanene/ML $\text{Cr}_2\text{Si}_2\text{Te}_6$ heterostructure, a

Hubbard U value of 4 eV was employed in our calculations. The similar rescale method is used to counteract the overestimation of T_C by MC simulations. Specifically, the calculated $T_C^{MC}(\text{Cr}_2\text{Si}_2\text{Te}_6)$ of 27 K for ML $\text{Cr}_2\text{Si}_2\text{Te}_6$ was scaled to the experimentally determined T_C^{exp} of 17 K for 2D $\text{Cr}_2\text{Si}_2\text{Te}_6$ [51]. As shown in Fig. 7(b), the germanene/ML $\text{Cr}_2\text{Si}_2\text{Te}_6$ heterostructure exhibits the QAHE up to 50 K under a 1.3% tensile strain.

V. DISCUSSION AND CONCLUSION

The QAHE temperature of materials cannot exceed its T_C and the topological band gap. For the MnBi_2Te_4 with band gap of 100-200 meV (≈ 1160 -2320 K) and T_C of 20 K, the upper limit of the QAHE temperature cannot exceed 20 K. For the germanene/ML $\text{Cr}_2\text{Ge}_2\text{Te}_6$ heterostructure with biaxial tensile strain, the upper limit of the QAHE temperature cannot exceed 62 K, as shown in Fig. 5. Thus, the higher upper limit of QAHE temperature in germanene/ML $\text{Cr}_2\text{Ge}_2\text{Te}_6$ heterostructure is expected larger than that in MnBi_2Te_4 .

The realization of the room-temperature QAH state requires two fundamental criteria: (i) a T_C exceeding 300 K, and (ii) a topological band gap larger than 300 K (≈ 26 meV). However, in practical materials implementations, these ideal conditions often remain unattainable. A representative example is MnBi_2Te_4 , where the QAH effect was experimentally observed at cryogenic temperatures (~ 1 -2 K), significantly below both its intrinsic T_C (~ 20 K) and the estimated band gap energy (100-200 meV) [12–14]. The experimental observation deviates from theoretical predictions and can be attributed to two principal factors: (1) extrinsic material imperfections such as structural disorders in samples, and (2) intrinsic magnetic fluctuations occurring below T_C that effectively suppress the QAH transition temperature.

The disorder effect can be categorized into two distinct types: magnetic disorder and nonmagnetic disorder. Many studies have revealed that weak magnetic disorder stabilizes the edge states and the QAH conductance, whereas strong disorder drives the system into an Anderson insulating phase [52–58]. The nonmagnetic disorder induces layer-dependent topological phase transitions. Weak disorder generally enhances the robustness of topological edge states and preserves the QAH con-

ductance. By increasing disorder, the quantization will also be disrupted [59, 60].

We applied in-plane biaxial tensile strain that preserves the space group symmetry of the system. The time-reversal symmetry is broken by the magnetic semiconductor in the heterostructure to realize the QAH state. Strain can effectively enhance Curie temperature T_C of some 2D ferromagnetic semiconductors, including $\text{Cr}_2\text{Ge}_2\text{Se}_6$ [42], MnSe_2 [61] and $\text{Fe}_2\text{Cl}_3\text{I}_3$ [62]. When these materials form heterostructures with topological insulators, it is highly expected that the QAH transition temperatures could be synergistically enhanced due to the strain-enhanced T_C .

We note that the quantum spin Hall (QSH) effect at room temperature has been demonstrated in Bi_4Br_4 [63]. In our paper, the QAH effect has been studied, which only has been observed in experiments at very low temperature so far. According to the results in our paper, it will be very interesting to explore the possible high temperature QAH effect in the heterostructures $\text{Bi}_4\text{Br}_4/\text{FS}$ (FS = ferromagnetic semiconductors).

In this paper, we have investigated the strain-enhanced QAHE in germanene/ML $\text{Cr}_2\text{Ge}_2\text{Te}_6$, germanene/BL $\text{Cr}_2\text{Ge}_2\text{Te}_6$ and germanene/ML $\text{Cr}_2\text{Si}_2\text{Te}_6$ heterostructures based on first principle calculations. Our calculations demonstrate the emergence of topologically nontrivial edge states and quantized anomalous Hall conductance in these heterostructures under tensile strain. We find that increasing tensile strain leads to an increase in T_C and a decrease in band gap within these germanene/magnetic semiconductor heterostructures. Consequently, the highest QAHE temperatures achieved are 62 K for the germanene/ML $\text{Cr}_2\text{Ge}_2\text{Te}_6$ heterostructure under 2.1% tensile strain, 64 K for the germanene/BL $\text{Cr}_2\text{Ge}_2\text{Te}_6$ heterostructure under 1.4% tensile strain, and 50 K for the germanene/ML $\text{Cr}_2\text{Si}_2\text{Te}_6$ heterostructure under 1.3% tensile strain. This work identifies experimental available materials for realizing high temperature QAHE states.

ACKNOWLEDGEMENTS

This work is supported by National Key R&D Program of China (Grant No. 2022YFA1405100), Chinese Academy of Sciences (Grants No. YSBR-030, No. JZHKYPT-2021-08).

-
- [1] F. D. M. Haldane, Model for a Quantum Hall Effect without Landau Levels: Condensed-Matter Realization of the "Parity Anomaly", *Phys. Rev. Lett.* **61**, 2015 (1988).
 - [2] D. J. Thouless, M. Kohmoto, M. P. Nightingale, and M. Den Nijs, Quantized Hall Conductance in a Two-Dimensional Periodic Potential, *Phys. Rev. Lett.* **49**, 405 (1982).

- [3] C.-Z. Chang, J. Zhang, X. Feng, J. Shen, Z. Zhang, M. Guo, K. Li, Y. Ou, P. Wei, L.-L. Wang, Z.-Q. Ji, Y. Feng, S. Ji, X. Chen, J. Jia, X. Dai, Z. Fang, S.-C. Zhang, K. He, Y. Wang, L. Lu, X.-C. Ma, and Q.-K. Xue, Experimental Observation of the Quantum Anomalous Hall Effect in a Magnetic Topological Insulator, *Science* **340**, 167 (2013).

- [4] C.-Z. Chang, W. Zhao, D. Y. Kim, H. Zhang, B. A. As-saf, D. Heiman, S.-C. Zhang, C. Liu, M. H. W. Chan, and J. S. Moodera, High-precision realization of robust quantum anomalous Hall state in a hard ferromagnetic topological insulator, *Nat. Mater.* **14**, 473 (2015).
- [5] J. G. Checkelsky, R. Yoshimi, A. Tsukazaki, K. S. Takahashi, Y. Kozuka, J. Falson, M. Kawasaki, and Y. Tokura, Trajectory of the anomalous Hall effect towards the quantized state in a ferromagnetic topological insulator, *Nat. Phys.* **10**, 731 (2014).
- [6] Y. Feng, X. Feng, Y. Ou, J. Wang, C. Liu, L. Zhang, D. Zhao, G. Jiang, S.-C. Zhang, K. He, X. Ma, Q.-K. Xue, and Y. Wang, Observation of the Zero Hall Plateau in a Quantum Anomalous Hall Insulator, *Phys. Rev. Lett.* **115**, 126801 (2015).
- [7] S. Grauer, S. Schreyeck, M. Winnerlein, K. Brunner, C. Gould, and L. W. Molenkamp, Coincidence of superparamagnetism and perfect quantization in the quantum anomalous Hall state, *Phys. Rev. B* **92**, 201304 (2015).
- [8] A. Kandala, A. Richardella, S. Kempinger, C.-X. Liu, and N. Samarth, Giant anisotropic magnetoresistance in a quantum anomalous Hall insulator, *Nat. Commun.* **6**, 7434 (2015).
- [9] X. Kou, S.-T. Guo, Y. Fan, L. Pan, M. Lang, Y. Jiang, Q. Shao, T. Nie, K. Murata, J. Tang, Y. Wang, L. He, T.-K. Lee, W.-L. Lee, and K. L. Wang, Scale-Invariant Quantum Anomalous Hall Effect in Magnetic Topological Insulators beyond the Two-Dimensional Limit, *Phys. Rev. Lett.* **113**, 137201 (2014).
- [10] X. Kou, L. Pan, J. Wang, Y. Fan, E. S. Choi, W.-L. Lee, T. Nie, K. Murata, Q. Shao, S.-C. Zhang, and K. L. Wang, Metal-to-insulator switching in quantum anomalous Hall states, *Nat. Commun.* **6**, 8474 (2015).
- [11] M. Mogi, R. Yoshimi, A. Tsukazaki, K. Yasuda, Y. Kozuka, K. S. Takahashi, M. Kawasaki, and Y. Tokura, Magnetic modulation doping in topological insulators toward higher-temperature quantum anomalous Hall effect, *Appl. Phys. Lett.* **107**, 182401 (2015).
- [12] Y. Deng, Y. Yu, M. Z. Shi, Z. Guo, Z. Xu, J. Wang, X. H. Chen, and Y. Zhang, Quantum anomalous Hall effect in intrinsic magnetic topological insulator MnBi_2Te_4 , *Science* **367**, 895 (2020).
- [13] C. Liu, Y. Wang, H. Li, Y. Wu, Y. Li, J. Li, K. He, Y. Xu, J. Zhang, and Y. Wang, Robust axion insulator and Chern insulator phases in a two-dimensional antiferromagnetic topological insulator, *Nat. Mater.* **19**, 522 (2020).
- [14] J. Ge, Y. Liu, J. Li, H. Li, T. Luo, Y. Wu, Y. Xu, and J. Wang, High-Chern-number and high-temperature quantum Hall effect without Landau levels, *Natl. Sci. Rev.* **7**, 1280 (2020).
- [15] C. Hu, L. Ding, K. N. Gordon, B. Ghosh, H.-J. Tien, H. Li, A. G. Linn, S.-W. Lien, C.-Y. Huang, S. Mackey, J. Liu, P. V. S. Reddy, B. Singh, A. Agarwal, A. Bansil, M. Song, D. Li, S.-Y. Xu, H. Lin, H. Cao, T.-R. Chang, D. Dessau, and N. Ni, Realization of an intrinsic ferromagnetic topological state in $\text{MnBi}_8\text{Te}_{13}$, *Sci. Adv.* **6**, eaba4275 (2020).
- [16] S. Tian, S. Gao, S. Nie, Y. Qian, C. Gong, Y. Fu, H. Li, W. Fan, P. Zhang, T. Kondo, S. Shin, J. Adell, H. Federwitz, H. Ding, Z. Wang, T. Qian, and H. Lei, Magnetic topological insulator $\text{MnBi}_6\text{Te}_{10}$ with a zero-field ferromagnetic state and gapped Dirac surface states, *Phys. Rev. B* **102**, 035144 (2020).
- [17] J.-Y. You, X.-J. Dong, B. Gu, and G. Su, Electric field induced topological phase transition and large enhancements of spin-orbit coupling and Curie temperature in two-dimensional ferromagnetic semiconductors, *Phys. Rev. B* **103**, 104403 (2021).
- [18] J.-Y. You, B. Gu, and G. Su, The p-orbital magnetic topological states on a square lattice, *Natl. Sci. Rev.* **9**, nwab114 (2022).
- [19] J.-Y. You, X.-J. Dong, B. Gu, and G. Su, Possible Room-Temperature Ferromagnetic Semiconductors, *Chin. Phys. Lett.* **40**, 067502 (2023).
- [20] R. Watanabe, R. Yoshimi, M. Kawamura, M. Mogi, A. Tsukazaki, X. Z. Yu, K. Nakajima, K. S. Takahashi, M. Kawasaki, and Y. Tokura, Quantum anomalous Hall effect driven by magnetic proximity coupling in all-telluride based heterostructure, *Appl. Phys. Lett.* **115**, 102403 (2019).
- [21] M. Serlin, C. L. Tschirhart, H. Polshyn, Y. Zhang, J. Zhu, K. Watanabe, T. Taniguchi, L. Balents, and A. F. Young, Intrinsic quantized anomalous Hall effect in a moiré heterostructure, *Science* **367**, 900 (2020).
- [22] A. L. Sharpe, E. J. Fox, A. W. Barnard, J. Finney, K. Watanabe, T. Taniguchi, M. A. Kastner, and D. Goldhaber-Gordon, Emergent ferromagnetism near three-quarters filling in twisted bilayer graphene, *Science* **365**, 605 (2019).
- [23] C. L. Tschirhart, M. Serlin, H. Polshyn, A. Shragai, Z. Xia, J. Zhu, Y. Zhang, K. Watanabe, T. Taniguchi, M. E. Huber, and A. F. Young, Imaging orbital ferromagnetism in a moiré Chern insulator, *Science* **372**, 1323 (2021).
- [24] T. Li, S. Jiang, B. Shen, Y. Zhang, L. Li, Z. Tao, T. Devakul, K. Watanabe, T. Taniguchi, L. Fu, J. Shan, and K. F. Mak, Quantum anomalous Hall effect from intertwined moiré bands, *Nature* **600**, 641 (2021).
- [25] W.-X. Qiu, B. Li, X.-J. Luo, and F. Wu, Interaction-Driven Topological Phase Diagram of Twisted Bilayer MoTe_2 , *Phys. Rev. X* **13**, 041026 (2023).
- [26] J. Zhu, J.-J. Su, and A. H. MacDonald, Voltage-Controlled Magnetic Reversal in Orbital Chern Insulators, *Phys. Rev. Lett.* **125**, 227702 (2020).
- [27] P. Bampoulis, C. Castenmiller, D. J. Klaassen, J. Van Mil, Y. Liu, C.-C. Liu, Y. Yao, M. Ezawa, A. N. Rudenko, and H. J. W. Zandvliet, Quantum Spin Hall States and Topological Phase Transition in Germanene, *Phys. Rev. Lett.* **130**, 196401 (2023).
- [28] F. Matusalem, M. Marques, L. K. Teles, L. Matthes, J. Furthmüller, and F. Bechstedt, Quantization of spin Hall conductivity in two-dimensional topological insulators versus symmetry and spin-orbit interaction, *Phys. Rev. B* **100**, 245430 (2019).
- [29] C. Gong, L. Li, Z. Li, H. Ji, A. Stern, Y. Xia, T. Cao, W. Bao, C. Wang, Y. Wang, Z. Q. Qiu, R. J. Cava, S. G. Louie, J. Xia, and X. Zhang, Discovery of intrinsic ferromagnetism in two-dimensional van der Waals crystals, *Nature* **546**, 265 (2017).
- [30] R. Zou, F. Zhan, B. Zheng, X. Wu, J. Fan, and R. Wang, Intrinsic quantum anomalous Hall phase induced by proximity in the van der Waals heterostructure germanene/ $\text{Cr}_2\text{Ge}_2\text{Te}_6$, *Phys. Rev. B* **101**, 161108 (2020).
- [31] H. Zhang, W. Qin, M. Chen, P. Cui, Z. Zhang, and X. Xu, Converting a two-dimensional ferromagnetic insulator into a high-temperature quantum anomalous Hall system by means of an appropriate surface modification,

- Phys. Rev. B **99**, 165410 (2019).
- [32] X.-J. Dong, J.-Y. You, Z. Zhang, B. Gu, and G. Su, Great enhancement of Curie temperature and magnetic anisotropy in two-dimensional van der Waals magnetic semiconductor heterostructures, *Phys. Rev. B* **102**, 144443 (2020).
 - [33] A. O'Neill, S. Rahman, Z. Zhang, P. Schoenherr, T. Yildirim, B. Gu, G. Su, Y. Lu, and J. Seidel, Enhanced Room Temperature Ferromagnetism in Highly Strained 2D Semiconductor $\text{Cr}_2\text{Ge}_2\text{Te}_6$, *ACS Nano* **17**, 735 (2023).
 - [34] Z. Ni, A. V. Haglund, H. Wang, B. Xu, C. Bernhard, D. G. Mandrus, X. Qian, E. J. Mele, C. L. Kane, and L. Wu, Imaging the Néel vector switching in the monolayer antiferromagnet MnPSe_3 with strain-controlled Ising order, *Nat. Nanotechnol.* **16**, 782 (2021).
 - [35] G. Krizman, J. Bermejo-Ortiz, T. Zakusylo, M. Hajaoui, T. Takashiro, M. Rosmus, N. Olszowska, J. J. Kołodziej, G. Bauer, Y. Guldner, G. Springholz, and L.-A. De Vaultier, Valley-Polarized Quantum Hall Phase in a Strain-Controlled Dirac System, *Phys. Rev. Lett.* **132**, 166601 (2024).
 - [36] T. M. G. Mohiuddin, A. Lombardo, R. R. Nair, A. Bonetti, G. Savini, R. Jalil, N. Bonini, D. M. Basko, C. Galotis, N. Marzari, K. S. Novoselov, A. K. Geim, and A. C. Ferrari, Uniaxial strain in graphene by Raman spectroscopy: G peak splitting, Grüneisen parameters, and sample orientation, *Phys. Rev. B* **79**, 205433 (2009).
 - [37] M. Šiškins, S. Kurdi, M. Lee, B. J. M. Slotboom, W. Xing, S. Mañas-Valero, E. Coronado, S. Jia, W. Han, T. van der Sar, H. S. J. van der Zant, and P. G. Steeneken, Nanomechanical probing and strain tuning of the Curie temperature in suspended $\text{Cr}_2\text{Ge}_2\text{Te}_6$ -based heterostructures, *npj 2D Mater. Appl.* **6**, 1 (2022).
 - [38] H. Zeng, H. Yu, B. Liu, S. Lu, X. Wei, L. Gao, M. Hong, X. Zhang, Z. Zhang, and Y. Zhang, Gradient-Strained Van Der Waals Heterojunctions for High-Efficient Photodetectors, *Adv. Funct. Mater.* **34**, 2400712.
 - [39] G. Kresse and J. Furthmüller, Efficient iterative schemes for *ab initio* total-energy calculations using a plane-wave basis set, *Phys. Rev. B* **54**, 11169 (1996).
 - [40] J. P. Perdew, K. Burke, and M. Ernzerhof, Generalized Gradient Approximation Made Simple, *Phys. Rev. Lett.* **77**, 3865 (1996).
 - [41] S. Grimme, J. Antony, S. Ehrlich, and H. Krieg, A consistent and accurate *ab initio* parametrization of density functional dispersion correction (DFT-D) for the 94 elements H-Pu, *J. Chem. Phys.* **132**, 154104 (2010).
 - [42] X.-J. Dong, J.-Y. You, B. Gu, and G. Su, Strain-Induced Room-Temperature Ferromagnetic Semiconductors with Large Anomalous Hall Conductivity in Two-Dimensional $\text{Cr}_2\text{Ge}_2\text{Se}_6$, *Phys. Rev. Appl.* **12**, 014020 (2019).
 - [43] A. A. Mostofi, J. R. Yates, Y.-S. Lee, I. Souza, D. Vanderbilt, and N. Marzari, Wannier90: A tool for obtaining maximally-localised Wannier functions, *Comput. Phys. Commun.* **178**, 685 (2008).
 - [44] A. A. Mostofi, J. R. Yates, G. Pizzi, Y.-S. Lee, I. Souza, D. Vanderbilt, and N. Marzari, An updated version of wannier90: A tool for obtaining maximally-localised Wannier functions, *Comput. Phys. Commun.* **185**, 2309 (2014).
 - [45] Q. Wu, S. Zhang, H.-F. Song, M. Troyer, and A. A. Soluyanov, WannierTools: An open-source software package for novel topological materials, *Comput. Phys. Commun.* **224**, 405 (2018).
 - [46] See supplemental material, .
 - [47] P. W. Anderson, New Approach to the Theory of Superexchange Interactions, *Phys. Rev.* **115**, 2 (1959).
 - [48] J. B. Goodenough, Theory of the Role of Covalence in the Perovskite-Type Manganites $[\text{La}, \text{M}(\text{II})]\text{MnO}_3$, *Phys. Rev.* **100**, 564 (1955).
 - [49] J. Kanamori, Crystal Distortion in Magnetic Compounds, *J. Appl. Phys.* **31**, S14 (1960).
 - [50] J. R. Schrieffer and P. A. Wolff, Relation between the Anderson and Kondo Hamiltonians, *Phys. Rev.* **149**, 491 (1966).
 - [51] C. Zhang, L. Wang, Y. Gu, X. Zhang, L.-L. Huang, Y. Fu, C. Liu, J. Lin, X. Zou, H. Su, J.-W. Mei, and J.-F. Dai, Layer-controlled Ferromagnetism in atomically thin CrSiTe_3 Flakes (2021), [arXiv:2111.05495 \[cond-mat\]](https://arxiv.org/abs/2111.05495).
 - [52] C.-Z. Chen, H. Liu, and X. C. Xie, Effects of Random Domains on the Zero Hall Plateau in the Quantum Anomalous Hall Effect, *Phys. Rev. Lett.* **122**, 026601 (2019).
 - [53] A. Haim, R. Ilan, and J. Alicea, Quantum Anomalous Parity Hall Effect in Magnetically Disordered Topological Insulator Films, *Phys. Rev. Lett.* **123**, 046801 (2019).
 - [54] E. O. Lachman, A. F. Young, A. Richardella, J. Cuppens, H. R. Naren, Y. Anahory, A. Y. Meltzer, A. Kandala, S. Kempinger, Y. Myasoedov, M. E. Huber, N. Samarth, and E. Zeldov, Visualization of superparamagnetic dynamics in magnetic topological insulators, *Sci. Adv.* **1**, e1500740 (2015).
 - [55] I. Lee, C. K. Kim, J. Lee, S. J. L. Billinge, R. Zhong, J. A. Schneeloch, T. Liu, T. Valla, J. M. Tranquada, G. Gu, and J. C. S. Davis, Imaging Dirac-mass disorder from magnetic dopant atoms in the ferromagnetic topological insulator $\text{Cr}_x(\text{Bi}_{0.1}\text{Sb}_{0.9})_{2-x}\text{Te}_3$, *Proc. Natl. Acad. Sci.* **112**, 1316 (2015).
 - [56] K. Nomura and N. Nagaosa, Surface-Quantized Anomalous Hall Current and the Magnetoelectric Effect in Magnetically Disordered Topological Insulators, *Phys. Rev. Lett.* **106**, 166802 (2011).
 - [57] Z. Qiao, Y. Han, L. Zhang, K. Wang, X. Deng, H. Jiang, S. A. Yang, J. Wang, and Q. Niu, Anderson Localization from the Berry-Curvature Interchange in Quantum Anomalous Hall Systems, *Phys. Rev. Lett.* **117**, 056802 (2016).
 - [58] W. Wang, Y. Ou, C. Liu, Y. Wang, K. He, Q.-K. Xue, and W. Wu, Direct evidence of ferromagnetism in a quantum anomalous Hall system, *Nat. Phys.* **14**, 791 (2018).
 - [59] T. Okugawa, P. Tang, A. Rubio, and D. M. Kennes, Topological phase transitions induced by disorder in magnetically doped $(\text{Bi,Sb})_2\text{Te}_3$ thin films, *Phys. Rev. B* **102**, 201405 (2020).
 - [60] Z.-Q. Zhang, C.-Z. Chen, Y. Wu, H. Jiang, J. Liu, Q.-f. Sun, and X. C. Xie, Chiral interface states and related quantized transport in disordered Chern insulators, *Phys. Rev. B* **103**, 075434 (2021).
 - [61] J.-W. Li, G. Su, and B. Gu, Possible room-temperature ferromagnetic semiconductor in monolayer MnSe_2 through a metal-semiconductor transition, *Phys. Rev. B* **109**, 134436 (2024).
 - [62] Z. Zhang, J.-Y. You, B. Gu, and G. Su, Antiferromagnetic and Electric Polarized States in Two-Dimensional Janus Semiconductor $\text{Fe}_2\text{Cl}_3\text{I}_3$, *J. Phys. Chem. C* **124**, 19219 (2020).
 - [63] N. Shumiya, M. S. Hossain, J.-X. Yin, Z. Wang, M. Litskevich, C. Yoon, Y. Li, Y. Yang, Y.-X. Jiang,

G. Cheng, Y.-C. Lin, Q. Zhang, Z.-J. Cheng, T. A. Cochran, D. Multer, X. P. Yang, B. Casas, T.-R. Chang, T. Neupert, Z. Yuan, S. Jia, H. Lin, N. Yao, L. Balicas, F. Zhang, Y. Yao, and M. Z. Hasan, Evidence of

a room-temperature quantum spin Hall edge state in a higher-order topological insulator, [Nat. Mater. **21**, 1111 \(2022\)](#).